

SUPPORTING INFORMATION

Rational Screening of Single-Atom-Doped ZnO Catalysts for Propane Dehydrogenation from Microkinetic Analysis

Fang Ma,^{a, §} Qing-Yu Chang,^{a, §} Qiang Yin,^a Zhi-Jun Sui,^a Xing-Gui Zhou,^a De Chen,^b Yi-An Zhu^{a,}*

^aUnited Chemical Reaction Engineering Research Institute (UNILAB), State Key Laboratory of Chemical Engineering, School of Chemical Engineering, East China University of Science and Technology, Shanghai 200237, China

^bDepartment of Chemical Engineering, Norwegian University of Science and Technology, N-7491 Trondheim, Norway

Author Contributions

§These authors contributed equally.

* Corresponding author: yanzhu@ecust.edu.cn (Yi-An Zhu)

S1. Calculated adsorption energies (in eV) of propylene before and after U_{eff} applied to doped single atoms on $\text{Mn}_1\text{-ZnO}$ and $\text{Cu}_1\text{-ZnO}$

Table S1. Calculated adsorption energies (in eV) of propylene on $\text{Mn}_1\text{-ZnO}$ and $\text{Cu}_1\text{-ZnO}$ with and without applying the effective U_{eff} to single atoms

Surface	Without application of U_{eff} to doped atoms	With application of U_{eff} to doped atoms	$\Delta E_{\text{ads,diff}}$
$\text{Mn}_1\text{-ZnO}$	-0.72	-0.72	0.00
$\text{Cu}_1\text{-ZnO}$	-0.52	-0.45	0.07

In this work, the effective U values are only applied to Zn. Determining an appropriate U_{eff} for the doped single metals on ZnO can be quite tricky. Typically, the U_{eff} values are obtained by fitting calculated band gap and thermodynamic quantities of bulk materials to available experimental data. Even by this, there is difficulty of ensuring that the fitting to one property can correctly reproduce others. In our case, the surface coverage of doped single atoms is very low, and it is even more difficult to find a physical property to make the fitting. Nevertheless, we have used the previously determined U_{eff} values for Mn and Cu (3.5 eV and 2.8 eV, respectively, as determined in J Phys: Condens Matter, 2019, 31, 145901) to see if the application of U to the doped single atoms would greatly influence the calculated energetics. The calculated adsorption energies of propylene on the $\text{Mn}_1\text{-ZnO}$ and $\text{Cu}_1\text{-ZnO}$ with and without applying the effective U to the single atoms are summarized in Table S1. From the table, we can see that the energy difference is less than 0.1 eV, which is within the uncertainty of DFT calculations. Therefore, we did not apply effective U values to the doped transition metals.

S2. Binding energies of Pt to Zn-deficient ZnO($10\bar{1}0$) at various Pt coverages

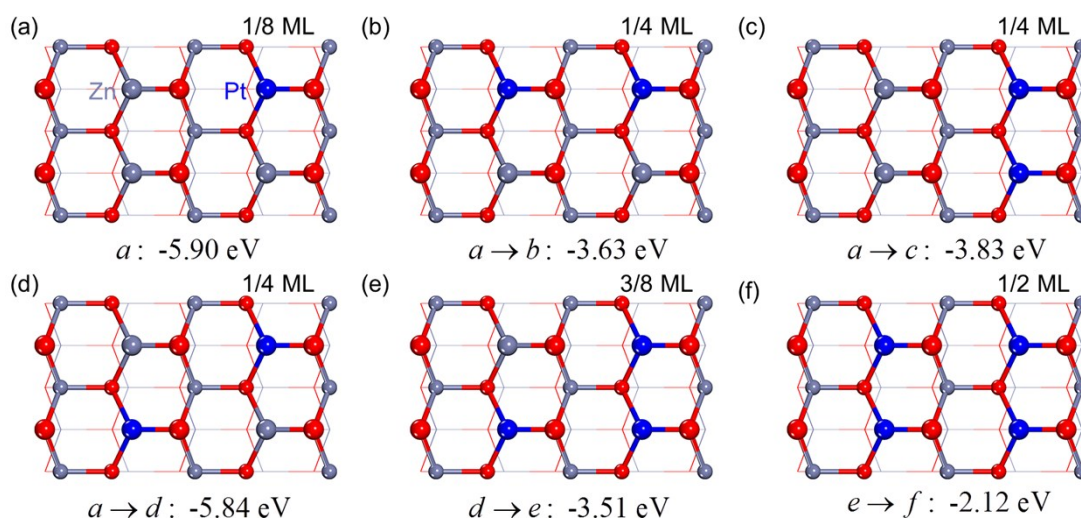


Fig. S1. Top views of Pt-doped ZnO($10\bar{1}0$) with successive substitution of Pt for Zn. The corresponding binding energies of Pt to the Zn-deficient surface are also given.

In the main text, we have demonstrated that, when one of the eight Zn atoms in the outermost layer of the $p(2 \times 2)$ supercell of ZnO($10\bar{1}0$) was replaced by other transition metals (at a coverage of 1/8 ML), almost all of them have a more negative binding energy than the cohesive energy. Given the uncertainty of DFT calculations (~ 0.2 eV), the single atoms of interest were predicted to stay atomically dispersed on the defective ZnO surface. The question that now arises is whether there exists a maximum possible coverage of the doped atoms beyond which a stable M_1 -ZnO($10\bar{1}0$) surface structure can no longer be retained. Taking Pt₁-ZnO as an example, we find that, if Pt atoms are successively substituted for Zn, the binding energy of Pt becomes less negative and would eventually be less negative than the cohesive energy of bulk Pt, as shown in Figure S1. In particular, when the Pt coverage is increased from 1/8 ML to 1/4 ML, there is one configuration available (see Fig. S1d) in which Pt has a more negative binding energy (-5.84 eV) than the cohesive energy (-5.08 eV), leading to a stable single-atom-doped surface. The close binding energy of Pt at the coverage of 1/8 ML (-5.90 eV) further indicates that substitution of one single atom at such a

coverage does not alter the physiochemical properties of its periodic replications. If we continue to substitute Pt for Zn at the Pt coverage of 3/8 ML [see Fig. S1e], however, the opposite is true; that is, sintering of Pt becomes energetically more favorable. Therefore, the maximum possible coverage of single Pt atoms on ZnO($10\bar{1}0$) is suggested to be 1/4 ML, which is high enough to play a role in determining the kinetics of PDH. This finding, on the other hand, explains why a $p(2 \times 2)$ supercell rather than a $p(1 \times 1)$ or a $p(2 \times 1)$ supercell should be used to represent the ZnO($10\bar{1}0$) surface in the present work.

S3. Charge compensation on Pt₁-ZnO and Mn₁-ZnO.

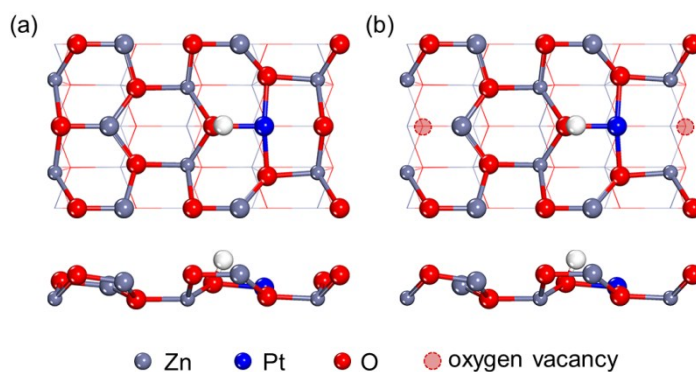


Fig. S2. Top and side views of (a) Pt₁-H/ZnO and (b) Pt₁-H/ZnO with an O vacancy.

To explore, in a systematic way, whether charge compensation is necessary for a reasonably accurate depiction of the adsorption property and behavior of the doped surfaces, we took Pt₁-ZnO and Mn₁-ZnO (on which Pt and Mn are low- and high-valence dopants, respectively) as two examples and calculated first the binding energy of the doped atoms and oxygen vacancy formation energy to assess the structural stability of the doped surfaces. These calculations were conducted with and without considering charge compensation, and comparisons have been made. Then, the electronic structure of the doped surfaces was characterized to account for the observed trend.

By performing the Bader charge analysis, it was demonstrated that most single atoms concerned in this work, except Mn, Fe, and Os, carry less positive charges than Zn on the pristine surface, causing the surfaces to be electron-deficient. Hu et al. (J Phys Chem C, 2011, 115, 3065) suggested the presence of a low-valence dopant in the outermost layer makes the doped oxides a better oxidant and adsorbing an electron donor on the surface would counteract the effect of the dopant. To see if this is the case for our systems of interest, the binding energy of the single Pt atom to the Zn-deficient surface with an H atom adsorbed at the O site adjacent to Pt (see Fig. S2a) was calculated. Here the H atom acts as an electron donor, and the calculated binding energy is -3.76 eV, which is much less negative than that without charge compensation (-5.90 eV) and even less negative than the

cohesive energy of bulk Pt (-5.08 eV); that is, compensating for charges has a negative effect on the stability of the Pt₁-doped surface, making the aggregation of Pt thermodynamically more favorable.

Oxygen vacancy formation energy is another quantity which is intimately related to the structural stability of oxide surfaces and is defined as

$$\Delta E_{f,vac} = E_{defective} + \frac{1}{2}E_{O_2} - E_{perfect}$$

where $E_{perfect}$ and $E_{defective}$ are the total energies of the pristine and oxygen-deficient surface, respectively, and E_{O_2} is the total energy of a free O₂ molecule in its triplet state. Under this definition, the more positive the $\Delta E_{f,vac}$, the less is the energy needed to form an oxygen vacancy, and hence the more stable is the doped surface. The oxygen vacancy that is formed on Pt₁-H/ZnO is shown schematically in Fig. S2b, and the calculated oxygen vacancy formation energies on Pt₁-ZnO and Pt₁-H/ZnO are listed in Table S2. From the table, we can see that the $\Delta E_{f,vac}$ becomes less positive when H is adsorbed on the surface to compensate for charges; that is, oxygen would be more readily removed from the surface and the oxide surface becomes less stable. To summarize, aggregation of Pt single atoms to form islands and creation of extra defects may occur more readily on Pt₁-H/ZnO upon charge compensation.

Table S2. Calculated binding energy ($\Delta E_{binding,M}$) and formation energy of oxygen vacancy ($\Delta E_{f,vac}$) on M₁-ZnO.

Energy (eV)	$\Delta E_{cohesive,M}$	$\Delta E_{binding,M}$	$\Delta E_{f,vac}$
Pt ₁ -ZnO	-5.08	-5.90	3.41
Pt ₁ -H/ZnO		-3.76	3.19
Mn ₁ -ZnO	-3.30	-7.71	4.04
Mn ₁ -(Zn _{vac})/ZnO		-7.67	3.63

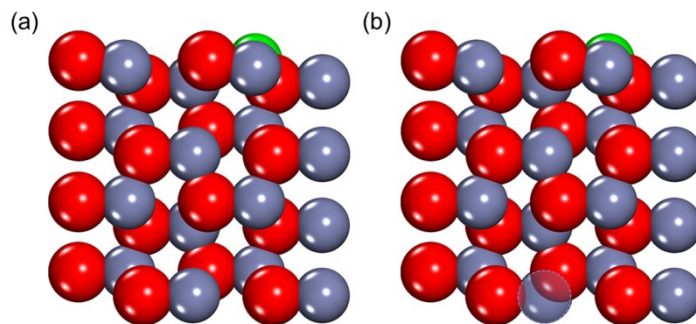


Fig. S3. Side views of (a) $\text{Mn}_1\text{-}/\text{ZnO}$ and (b) $\text{Mn}_1\text{-(Zn}_{\text{vac}})\text{/ZnO}$.

Similarly, the calculations have been performed on $\text{Mn}_1\text{-ZnO}$ where a high-valence dopant is present. On such a surface, the slab carries excessive electrons. For this reason, in addition to the Zn atom that is replaced with Mn, a Zn atom on the rear surface of the slab is abstracted from the system to create an extra point defect, as shown in Figure S3. It is found that the binding energy of Mn to the Zn-deficient surface becomes a little less negative, changing from -7.71 eV to -7.67 eV. Meanwhile, the calculated oxygen vacancy formation energy becomes less positive. The data have also been given in Table S2. These results indicate that compensating for charges on the $\text{Mn}_1\text{-ZnO}(10\bar{1}0)$ surface has a negligible or negative effect on the structural stability as well.

The reason charge compensation cannot give rise to a more stable slab, as least in our case, is that the charge transfer between transition metal and oxygen is far less complete. For example, Mn, Zn, and Pt exist on the surface in a $+1.31$, $+1.18$, and $+0.70$ oxidation state (see Table S3 below), respectively, which are much less than the formal oxidation states. Considering the low surface coverage of the doped single atoms, compensating charge by adsorbing H and creating extra Zn vacancy would overstate the charge imbalance arising from substitution of other transition metals for Zn.

Table S3. Effective Bader charges of M and electrons transferred on the single-atom-doped surfaces

Surface	M	Effective Bader charge on M ($ e $)	$\Delta q e ^a$		
			O_1	O_2	O_3
pristine ZnO	-	+1.18	-	-	-
M ₁ -ZnO(10 $\bar{1}$ 0)	Mn	+1.31	-0.02	-0.05	-0.01
	Fe	+1.21	+0.02	-0.03	+0.00
	Co	+1.08	+0.07	-0.01	+0.00
	Ni	+0.92	+0.14	+0.04	+0.00
	Cu	+0.96	+0.11	+0.02	+0.00
	Ru	+1.07	+0.11	+0.05	+0.00
	Rh	+0.86	+0.12	+0.08	+0.01
	Pd	+0.72	+0.15	+0.10	+0.02
	Ag	+0.75	+0.22	+0.05	+0.01
	Os	+1.19	+0.14	+0.07	+0.01
	Ir	+0.81	+0.13	+0.10	+0.02
	Pt	+0.70	+0.15	+0.11	+0.03
	Au	+0.61	+0.21	+0.12	+0.03

^a The positive and negative values signify an electron-loss and an electron-gain process, respectively.

S4. Calculated adsorption energies (in eV) of reaction intermediates on single-atom-doped ZnO

Table S4. Calculated adsorption energies (in eV) of reaction intermediates on single-atom-doped ZnO

Surface	Propane	H ₂	Propylen e	2-propyl	H	H&H	2- propyl&H
						M-O	M-O
Mn ₁ -ZnO	-0.32	-0.14	-0.32	-1.54	-2.26	-4.71	-3.76
Fe ₁ -ZnO	-0.28	-0.05	-0.83	-0.98	-1.32	-4.43	-3.51
Co ₁ -ZnO	-0.29	-0.07	-0.77	-1.47	-1.76	-4.70	-3.76
Ni ₁ -ZnO	-0.29	-0.05	-0.44	-1.14	-2.17	-4.55	-3.48
Cu ₁ -ZnO	-0.30	-0.08	-0.52	-1.11	-3.10	-4.77	-4.07
Ru ₁ -ZnO	-0.24	-0.04	-1.15	-1.84	-2.40	-4.74	-4.26
Rh ₁ -ZnO	-0.25	-0.04	-1.32	-1.86	-2.06	-5.18	-4.57
Pd ₁ -ZnO	-0.31	-0.05	-1.03	-1.74	-3.31	-5.23	-4.86
Ag ₁ -ZnO	-0.29	-0.07	-0.78	-1.49	-4.25	-5.31	-4.90
Os ₁ -ZnO	-0.28	-0.04	-1.27	-1.81	-1.74	-4.55	-4.11
Ir ₁ -ZnO	-0.27	-0.05	-1.53	-1.90	-2.50	-4.89	-4.47
Pt ₁ -ZnO	-0.26	-0.05	-1.30	-1.72	-2.59	-5.04	-4.78
Au ₁ -ZnO	-0.28	-0.06	-1.34	-2.11	-3.91	-6.19	-5.48

S5. Adsorption configurations of reaction intermediates on M_1 -ZnO

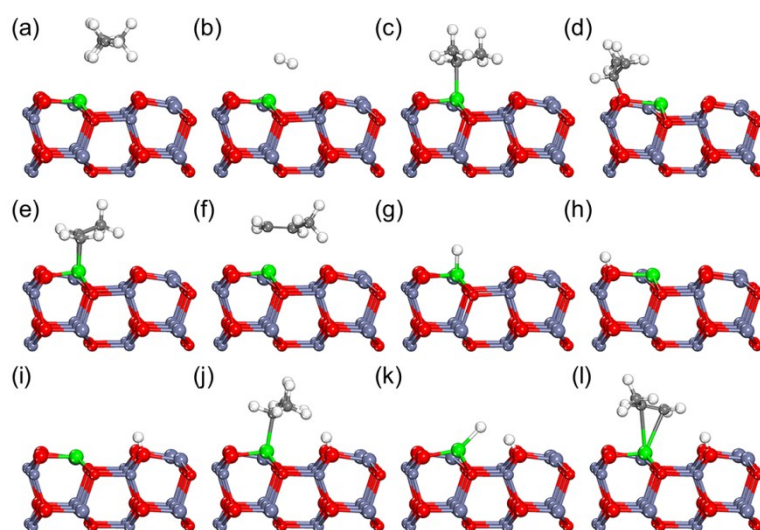


Fig. S4. Adsorption configurations of (a) propane, (b) hydrogen, (c, d) 2-propyl, (e, f) propylene, (g, h, i) hydrogen, (j) 2-propyl&H, (k) H&H, and (l) propylene&H on M_1 -ZnO.

S6. Decomposition of H&H coadsorption energy at the Zn₁-O₁ and Zn₁-O₃ sites and effective Bader charge on adsorbed species on ZnO

Table S5. Decomposition of H&H coadsorption energy at Zn₁-O₁ and Zn₁-O₃ sites and effective Bader charge on adsorbed species on ZnO.

Site	H+H	H&H	$\Delta E_{\text{int,acid-base}}$	$q_{\text{H+H}}(e)$		$q_{\text{H&H}}(e)$	
				M Site	O Site	M Site	O Site
Zn ₁ -O ₁	-4.12	-5.03	-1.60	-0.27	0.52	-0.39	0.53
Zn ₁ -O ₃	-4.12	-4.78	-2.71	-0.27	0.52	-0.43	0.56

S7. Decomposition of ΔE_{co-ads}

1. The adsorption energy of a Lewis acid and a Lewis base coadsorbed on an oxide surface can be calculated as (see Eq. 5 in the main text)

$$\Delta E_{co-ads} = E_{surf+acid+base} - E_{surf} - E_{acid} - E_{base}$$

where $E_{surf+acid+base}$, E_{surf} , E_{acid} , and E_{base} are the total energies of the oxide surface with the acid and base coadsorbed, the bare surface, gas-phase acid and base, respectively.

2. The Lewis acid-base interaction ($\Delta E_{int,acid-base}$) is essentially an electronic effect that arises purely from electron transfer. Any contributions from surface and adsorbate distortion should be differentiated from the ligand effect. Hence, a straightforward way to express the Lewis acid-base interaction is to express it as a difference in the bonding energy between coadsorption and individual adsorption:

$$\Delta E_{int,acid-base} = \Delta E_{bonding,acid+base} - \Delta E_{bonding,acid}^{constrained} - \Delta E_{bonding,base}^{constrained}$$

where $\Delta E_{bonding,acid+base}$ is the bonding energy that measures the strength of the direct interaction between the distorted surface and distorted species and can be calculated as

$$\Delta E_{bonding,acid+base} = E_{surf+acid+base} - E_{surf}^{constrained} - E_{acid}^{constrained} - E_{base}^{constrained}$$

where $E_{surf}^{constrained}$, $E_{acid}^{constrained}$, and $E_{base}^{constrained}$ are the total energies of the bare surface, isolated acid, and base with the geometries constrained to those upon coadsorption. These energies can be obtained from DFT single-point energy calculations, and the constrained structures are derived from the optimized structures of the surface with the acid and base coadsorbed on the surface.

$\Delta E_{bonding,acid}^{constrained}$ and $\Delta E_{bonding,base}^{constrained}$ are the bonding energies of the acid and base, respectively, with the geometries of the adsorbates and surface constrained to those upon coadsorption, which can be expressed as

$$\Delta E_{\text{bonding,acid}}^{\text{constrained}} = E_{\text{surf+acid}}^{\text{constrained}} - E_{\text{surf}}^{\text{constrained}} - E_{\text{acid}}^{\text{constrained}}$$

and

$$\Delta E_{\text{bonding,base}}^{\text{constrained}} = E_{\text{surf+base}}^{\text{constrained}} - E_{\text{surf}}^{\text{constrained}} - E_{\text{base}}^{\text{constrained}}$$

where $E_{\text{surf+acid}}^{\text{constrained}}$ and $E_{\text{surf+base}}^{\text{constrained}}$ are the total energies of the surfaces with the acid and base adsorbed in the geometries upon coadsorption. Consequently, we have

$$\Delta E_{\text{int,acid-base}} = E_{\text{surf+acid+base}} + E_{\text{surf}}^{\text{constrained}} - E_{\text{surf+acid}}^{\text{constrained}} - E_{\text{surf+base}}^{\text{constrained}}$$

3. $\Delta E_{\text{ads,acid}}^{\text{constrained}}$ and $\Delta E_{\text{ads,base}}^{\text{constrained}}$ are the adsorption energies of the acid and base when the geometries of the adsorption configurations are constrained to geometries upon coadsorption, which can be written as

$$\Delta E_{\text{ads,acid}}^{\text{constrained}} = E_{\text{surf+acid}}^{\text{constrained}} - E_{\text{surf}} - E_{\text{acid}}$$

and

$$\Delta E_{\text{ads,base}}^{\text{constrained}} = E_{\text{surf+base}}^{\text{constrained}} - E_{\text{surf}} - E_{\text{base}}$$

4. The equations above can be combined to give Eq. 6 in the main text:

$$\begin{aligned} \Delta E_{\text{co-ads}} &= E_{\text{surf+acid+base}} - E_{\text{surf}} - E_{\text{acid}} - E_{\text{base}} \\ &= E_{\text{surf+acid+base}} + E_{\text{surf}}^{\text{constrained}} - E_{\text{surf+acid}}^{\text{constrained}} - E_{\text{surf+base}}^{\text{constrained}} + E_{\text{surf}} - E_{\text{surf}}^{\text{constrained}} + E_{\text{surf+acid}}^{\text{constrained}} - E_{\text{surf}} - E_{\text{acid}} + E_{\text{surf+base}}^{\text{constrained}} - E_{\text{surf}} - E_{\text{base}} \\ &= \left(E_{\text{surf+acid+base}} + E_{\text{surf}}^{\text{constrained}} - E_{\text{surf+acid}}^{\text{constrained}} - E_{\text{surf+base}}^{\text{constrained}} \right) + \left(E_{\text{surf}} - E_{\text{surf}}^{\text{constrained}} \right) + \left(E_{\text{surf+acid}}^{\text{constrained}} - E_{\text{surf}} - E_{\text{acid}} \right) + \left(E_{\text{surf+base}}^{\text{constrained}} - E_{\text{surf}} - E_{\text{base}} \right) \\ &= \Delta E_{\text{int,acid-base}} - \Delta E_{\text{distortion,surf}} + \Delta E_{\text{ads,acid}}^{\text{constrained}} + \Delta E_{\text{ads,base}}^{\text{constrained}} \end{aligned}$$

where $\Delta E_{\text{distortion,surf}}$ is the distortion energy of the surface and equals the difference in the energy of the surface before and after coadsorption of the acid and base:

$$\Delta E_{\text{distortion,surf}} = E_{\text{surf}}^{\text{constrained}} - E_{\text{surf}}$$

S8. Decomposition of H&H coadsorption energy and effective Bader charge on adsorbed species on M₁-ZnO

Table S6. Decomposition of H&H coadsorption energy and effective Bader charge on adsorbed species on M₁-ZnO.

Surface	H+H	H&H	$\Delta E_{(H\&H)-(H+H)}$	$q_{H+H}(e)$		$q_{H\&H}(e)$	
				M Site	O Site	M Site	O Site
Mn ₁ -ZnO	-4.24	-4.71	-0.47	-0.32	0.51	-0.52	0.55
Fe ₁ -ZnO	-3.19	-4.43	-1.24	-0.38	0.51	-0.48	0.56
Co ₁ -ZnO	-3.58	-4.70	-1.12	-0.12	0.52	-0.44	0.56
Ni ₁ -ZnO	-3.56	-4.55	-0.99	-0.09	0.52	-0.41	0.55
Cu ₁ -ZnO	-3.98	-4.77	-0.79	-0.18	0.52	-0.35	0.55
Ru ₁ -ZnO	-4.75	-4.74	0.01	-0.14	0.52	-0.37	0.55
Rh ₁ -ZnO	-4.36	-5.18	-0.82	-0.10	0.52	-0.15	0.53
Pd ₁ -ZnO	-5.12	-5.23	-0.11	0.00	0.55	-0.19	0.55
Ag ₁ -ZnO	-5.53	-5.31	0.22	0.04	0.52	-0.23	0.54
Os ₁ -ZnO	-4.16	-4.55	-0.39	-0.13	0.52	-0.21	0.55
Ir ₁ -ZnO	-5.02	-4.89	0.13	-0.04	0.53	-0.13	0.53
Pt ₁ -ZnO	-4.65	-5.04	-0.39	0.01	0.53	-0.05	0.52
Au ₁ -ZnO	-6.35	-6.19	0.16	0.04	0.52	-0.16	0.54

S9. Computed charge density difference for coadsorption of H&H on single-atom-doped surfaces

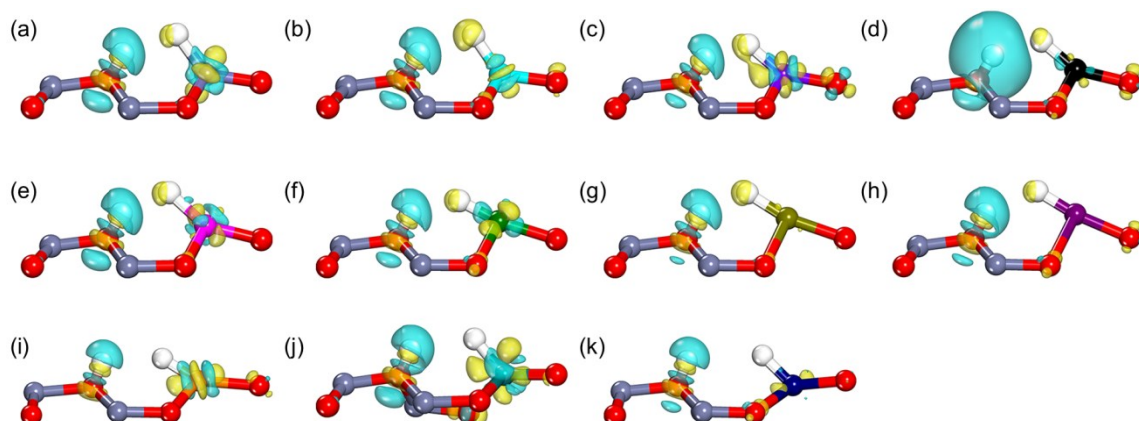


Fig. S5. Side views of the computed charge density difference for coadsorption of H&H on (a) Fe₁-ZnO, (b) Co₁-ZnO, (c) Ni₁-ZnO, (d) Cu₁-ZnO, (e) Ru₁-ZnO, (f) Pd₁-ZnO, (g) Ag₁-ZnO, (h) Au₁-ZnO, (i) Rh₁-ZnO, (j) Os₁-ZnO, and (k) Ir₁-ZnO. Charge accumulation and depletion are colored yellow and cyan, respectively, with the isosurface value being 0.05 e/Å³.

S10. Energy profiles for the 1st dehydrogenation step of propane on the pristine surface

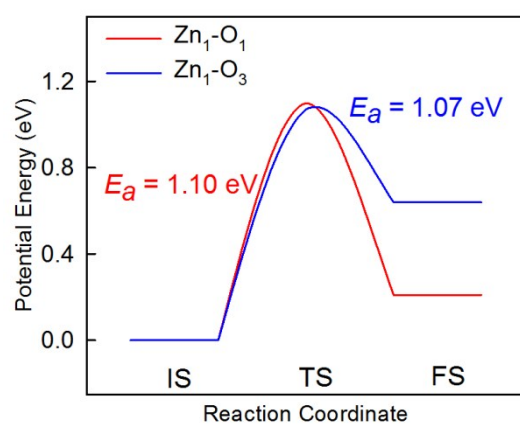


Fig. S6. Energy profiles for the first dehydrogenation step of propane on the pristine surface.

S11. Formation energy approach

In principle, formation energies should be computed by using a “reference state” for each element present in the gas-phase species, adsorbed species, and activated complex in the reaction. One advantage of the formation energy approach is that it does not distinguish between adsorbate states and transition states and their formation energies can be calculated relative to the same set of “atomic reference energies”. Because this approach ensures thermodynamic consistency, the use of formation energies as inputs to a kinetic model is preferred over other relative quantities such as adsorption, reaction, and activation energies. Here the total energies of free H₂ (U_{H_2}) and C₃H₈ ($U_{C_3H_8}$) were used to calculate the “atomic reference energies” of H (R_H) and C (R_C):

$$R_H = 0.5 \cdot U_{H_2}$$

$$R_C = (U_{C_3H_8} - 8R_H) / 3$$

For a gaseous species i , the formation energy was calculated as

$$E_i = U_i - \sum_j n_j R_j$$

where U_i is the total energy of species i and n_j is the number of the atomic species j in species i .

For an adsorbed species i , the formation energy was calculated as

$$E_i = U_i - U_{surf} - \sum_j n_j R_j$$

where U_{surf} is the total energy of the corresponding bare surface.

For example, the formation energy of adsorbed 2-propyl ($E_{CH_3CHCH_3^*}$) can be calculated as

$$E_{CH_3CHCH_3^*} = U_{surf+CH_3CHCH_3} - U_{surf} - 3R_C - 7R_H$$

where $U_{surf+CH_3CHCH_3}$ is the total energy of the metal-oxide surface with 2-propyl adsorbed.

S12. Plot of the calculated formation energies of 2-propyl against the formation energies of H

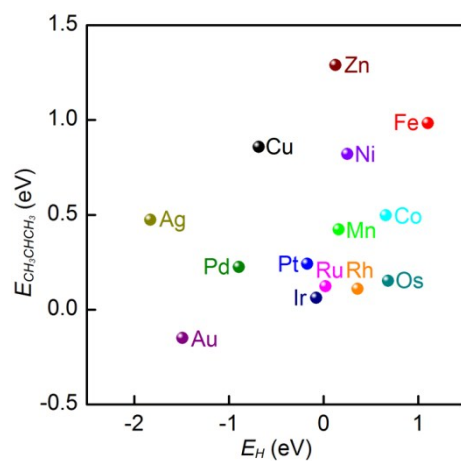


Fig. S7. Plot of the calculated formation energies of 2-propyl against the formation energies of H.

S13. Calculated formation energies of the transition states for dehydrogenation of 2-propyl as a function of the formation energies of H and 2-propyl

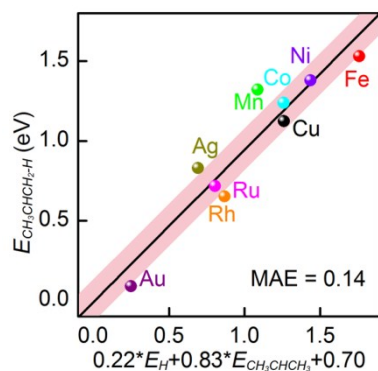


Fig. S8. Calculated formation energies of the transition states for dehydrogenation of 2-propyl as a function of the formation energies of H and 2-propyl.

S14. Coverages of reaction intermediates

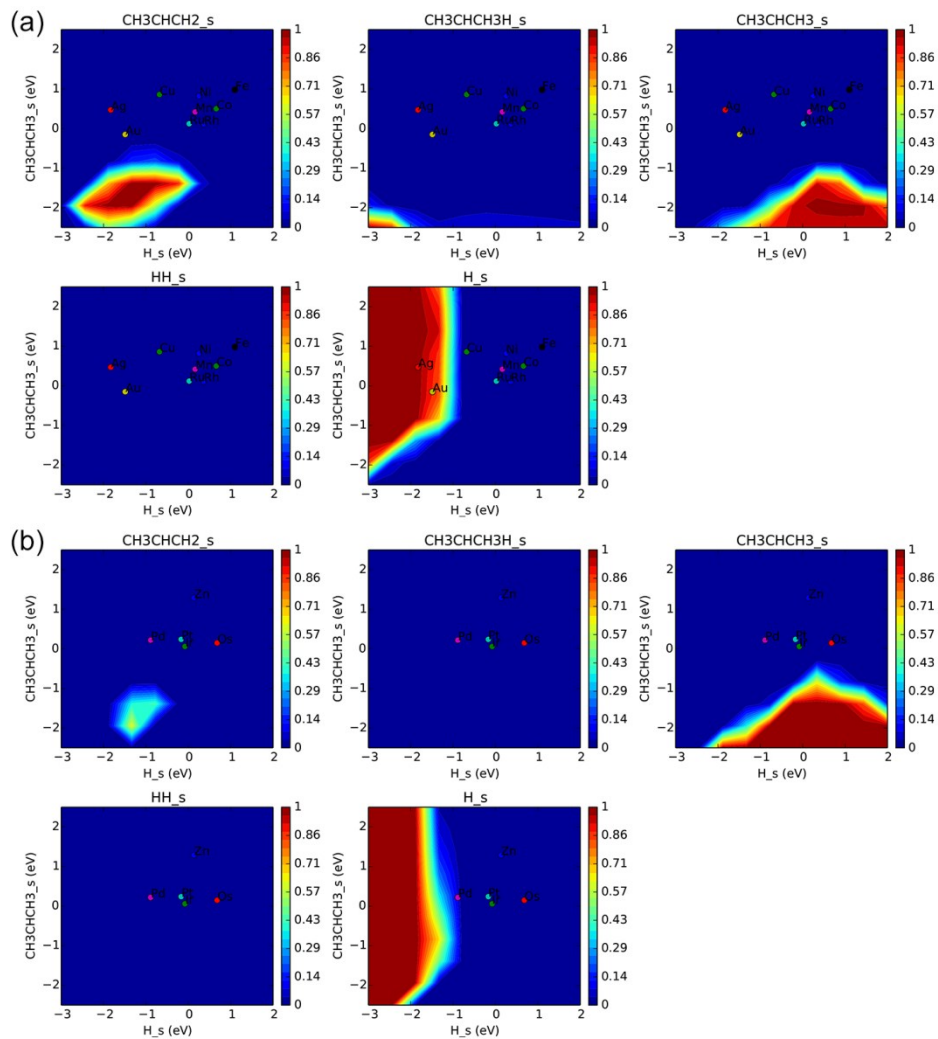


Fig. S9. Coverages of reaction intermediates on single-atom-doped ZnO(10 $\bar{1}0$).